ELSEVIER

Polymer 40 (1999) 4229–4236

polymer

Small molecule penetrant diffusion in aromatic polyesters: a molecular dynamics simulation study

Rishikesh K. Bharadwaj, Richard H. Boyd*

Departments of Materials Science and Engineering and of Chemical and Fuels Engineering, University of Utah, Salt Lake City, UT 84112, USA

Received 26 August 1998; received in revised form 1 September 1998; accepted 10 September 1998

Abstract

Molecular dynamics (MD) simulations have been used to study diffusion of methane in three highly impermeable aromatic polyesters that are good barrier materials. These are amorphous poly(ethylene terephthalate) (PET) and poly(ethylene 2,6-naphthalene dicarboxylate) (PEN), and the nematic mesophase of the thermotropic liquid crystalline copolyester (LCP) of *p*-hydroxy benzoic acid (HBA) and 2,6 hydroxy naphthoic acid (HNA). Diffusion coefficients were determined in the temperature ranges of 450–625 K for PET, 500–625 for PEN, 425–530 K for the LCP, where values are large enough to be accessible to MD in practical computation times. Extrapolation, via Arrhenius plots, of the coefficients to near room temperature gave good agreement with experimental data in that region. This was found even though the glass transition temperatures (T_g) of PET (350 K) and PEN (390 K) lie in the intervening temperature range. This finding confirms previous observations that a low temperature hopping regime for small penetrants sets in on cooling well before the T_g of the host. Analysis of diffusant trajectories in terms of diffusive jump size distribution also shows that the low temperature hopping regime remains in place over the temperature range studied in these low diffusion coefficient polymers. Correlation of diffusion coefficients with free volume was examined. The LCP, even though diffusion there is highly anisotropic, is found to lie on a correlation found previously for five other polymers studied via MD. However, PET and PEN fail badly and are found to diffuse much more slowly than inferred from free volume vs diffusion coefficient behavior in the other polymers.

Keywords: Liquid crystalline polymer; Vectra®; PET

1. Introduction

Transport of molecules in polymeric matrices is an important topic in the field of polymer science and technology [1]. One important reason for this interest is that polymeric materials find extensive application as barriers to the diffusion of gases. It has been shown recently that atomistic level simulations using the molecular dynamics (MD) technique can successfully compute diffusion coefficients of such penetrant molecules in a variety of bulk polymers [1–8]. This capability has proven to be very valuable in achieving understanding of the mechanism of diffusion and the relation between chemical architecture and rate of diffusion.

The mechanism of diffusion of small penetrants such as gas molecules deduced from simulation is interesting. At low temperature, the penetrant is trapped for long periods of time in a cage formed by the polymer matrix. The penetrant advances via a hopping mechanism from an old cage to a new one formed nearby [6,10]. As temperature increases, the mechanism gradually changes [6,7,9]. Jumps are more frequent and the time spent in the cages decreases in relative importance to the total time trajectory. At high temperature, the cage effect essentially disappears in favor of a liquid–like scattering process. Accompanying this effect, the activation energy, which at lower temperature behaves in Arrhenius fashion over a considerable region, decreases to a fraction of the low temperature value. Interestingly, the establishment of the low temperature Arrhenius regime takes place on cooling well above the glass transition region of the matrix and persists on lowering temperature into the glassy region.

As an example of structure vs diffusion insights, penetrant (methane) diffusion in polyisobutylene (PIB), where rates are comparatively slow, has been studied via simulation [5,6] and compared to that in polyethylene (PE) [6] and atactic polypropylene (aPP) [7]. The slow diffusion in PIB could be attributed to the larger chain cross-sectional area giving rise to more efficient packing and smaller free volume [6]. Further tests of the free volume concept have

* Corresponding author. Tel.: +1-801-581-6865; Fax: +1-801-581-4816.

E-mail address: boyd@poly2.mse.utah.edu (R.H. Boyd)

0032-3861/99/$ - see front matter
PII: S0032-3861(98)00671-5

been carried out. Diffusion in atactic polystyrene (aPS) [8] and *cis*-poly(butadiene) (PBD) [9] has also been studied and found to correlate well with fractional free volume.

In the present work, small penetrant diffusion simulation studies are extended to a class of structurally more complicated polymers, that is, to three aromatic polyesters. They are polymers in which the diffusion coefficients are smaller than in the systems previously mentioned and are excellent barrier materials. Two of the polymers are aromatic diacid esters with ethylene glycol, and are amorphous poly(ethylene terephthalate) (PET) and amorphous poly(ethylene 2,6-naphthalene dicarboxylate) (PEN). The third is a random copolymer of *p*-hydroxybenzoic (BA) acid and 2-hydroxy-6-naphthoic acid (HNA). The latter is a thermotropic liquid crystalline polymer (LCP) known commercially as Vectra®. This example is interesting since the chains are organized as parallel bundles over domains. The diffusion is expected to be highly anisotropic within these domains.

Two of the polymers, PET [11] and 70/30 HBA/HNA Vectra [12], have been the subject of previous simulations and the models are used directly in this work. Simulation of PEN is carried out here for the first time. Methane continues to be the choice for the penetrant, a selection originally made on the basis of its being well represented as a single centre and also as the largest of the gases commonly represented in this manner.

2. Simulation details

2.1. PET and PEN representation

PET was modeled with a single chain of 60 monomeric units packed in a cubic periodic simulation cell. The methylene (CH_2) units and the aromatic ring (C–H) units are modeled as anisotropic united atom (AUA) groups. The details and force field have been described previously [11].

PEN used the same group representations and energy model as PET and the simulation system also consisted of 60 monomeric units in a cubic periodic cell. In simulation studies of dynamic processes like diffusion that are sensitive to free volume it is important that the system volume be consistent not only with experiment but also with the desired pressure (1 atm in the case here) [2]. Thus, investigation of the PVT properties or equation of state is important. Such results for PET were reported and in fact nonbonded parameter adjustment for the united atom aromatic C–H units was based in part on matching the experimental melt density and thermal expansion [11]. The equation state was also investigated here for PEN. Volumes were established under constant particle number, N, pressure, P, and temperature, T, (NPT) dynamics at several temperatures at 1 atm. Also volume vs pressure at one temperature was determined via NPT dynamics. Since there is no parameter adjustment carried out here for PEN these PVT results are entirely predictive. Cohesive energy density was also computed at the same temperatures employed for the V–T investigation. The cohesive energy was found as the intermolecular portion of the nonbonded and electrostatic energies.

2.2. Vectra representation

The system studied and the force field parameters used have also been described in detail [12]. Briefly, the system consisted of 12 chains of 10 monomeric units (7 BA and 3 NA) each. The BA and NA units were randomly concatenated in each chain. All atoms including hydrogen were explicitly modeled. The periodic cell was orthorhombic in shape with independently adjustable a, b, c dimensions.

2.3. PET and PEN diffusion details

For PET a single methane penetrant was used to determine the mean square displacements at five temperatures, 625, 575, 525, 500 and 450 K. The simulations were between 1.5 to 2.5 ns in duration. The initial configurations were obtained from NPT simulations which were on the order of 1 ns in duration. The penetrants were introduced into the simulation box of dimensions determined in the volume equilibration step. Equilibration times were on the order of 250 ps at 625 and 575 K, 500 ps at 525 and 500 K and 1 ns at 450 K. For PEN the conditions were the same except that the 450 K temperature was excluded.

2.4. Vectra diffusion details

Three methane penetrants were inserted into equilibrated configurations generated by NPT dynamics. The equilibration was judged by the observation of the specific volume during the course of the simulation. The diffusion runs were performed under NVT conditions by fixing the volume to the equilibrated value found from NPT dynamics. The diffusants were inserted in the following manner. The orthorhombic periodic cell is quite elongated in the c or chain direction ($\sim$ 70 Å) relative to the lateral a, b dimensions ($\sim$ 14, 18 Å). The cell was considered to be sub-divided into three compartments along the c axis. A free volume or cavity search was conducted in each compartment via insertion of a large number of probe spheres. A penetrant was inserted at one of the larger cavities in the interior of each compartment and such that none of the penetrants were placed very close to each other. The mean square displacements were accumulated at four temperatures, 530, 500, 450 and 425 K. The runs were between 2–3 ns in duration with 500 ps equilibration time allowed to elapse after insertion of the penetrants before data collection. Although the chains have considerable translational freedom along the c direction, their ends tend to be congregated in the vicinity of the c axis cell faces creating an ‘end-zone’ region of looser packing [12]. At the higher temperatures, the penetrants placed in the compartments towards the chain ends tended to eventually move into the end-zone of the simulation cell. A

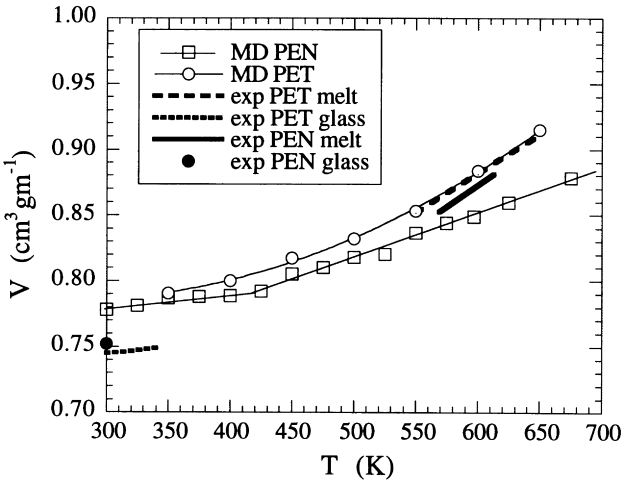

Fig. 1. Volume vs temperature for PEN at 1 atm as determined here from NPT dynamics (open squares, thin curve). Experimental data in the melt for PEN, is shown as a heavy line [13] and a single point for the glass is given (filled circle) [14]. Also shown is previous MD simulation data for PET (open circles, thin line) [11], experimental data for PET melt (heavy dashed line) [15] and experimental data for PET glass (heavy dotted line) [16].

penetrant was excluded from participation in the diffusion trajectory if it was within 5 Å of the end-zone. At 450 and 425 K, the mean square displacement data for all three penetrants could be used.

2.5. Free volume computation

The most simple and direct measure of free volume of the polymeric matrix is based on the volume unoccupied by the atom diameters, σ, at which the nonbonded potentials cross zero. This can be established by a 3-D mesh of insertion points or, as was done here, by inserting a large number of points randomly in the simulation box. A given point is either inside the σ diameter of at least one atom or is in the unoccupied free volume space. In addition, a point in free volume space has a distance to the closest σ sphere. This establishes the radius of the largest sphere that can be inserted at that point in unoccupied space. That space is also available to all spheres of smaller radii. Thus the fractional free volume and the fractional volume available to a sphere of given radius is computed from finding the atom neighbors of a large number of inserted points. This computation was carried out here for all three polymers equilibrated at 400 K. The temperature was selected to coincide with similar computations carried out previously [6–9].

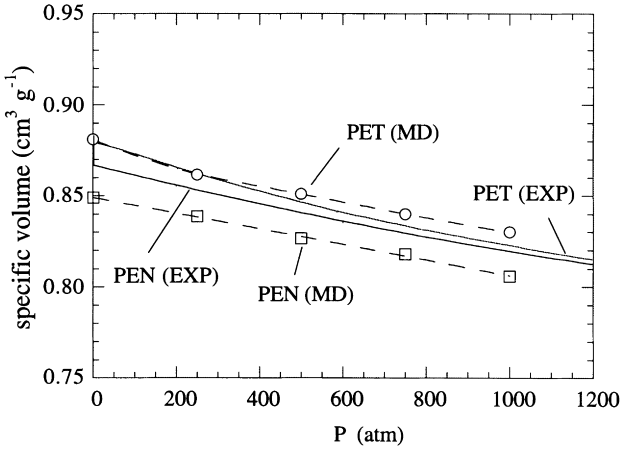

Figure 2. Volume vs pressure (at 597 K) for PEN from MD simulation (open squares, dashed curve). Previous MD results for PET [11] are shown as open circles, dashed curve. Experimental results for both PET and PEN are shown as the labeled solid curves [13,15].

3. Results and discussion

3.1. PVT behavior of PEN

Since, as indicated in Section 1, PEN has not been considered in simulation before, equation of state results are presented here. Fig. 1 displays the volume vs. temperature at 1 atm for PEN determined via NPT dynamics over a wide temperature range. Experimental data for the melt [13], and a single point for the room temperature glass [14] are shown as well. Also shown for comparison, are previous MD results for PET [11] along with appropriate experimental data [15,16]. It can be seen that the MD melt volume for PEN is fairly close to but noticeably lower than the experimental values. More serious is the observation that the thermal expansion coefficient is considerably less than the experimental. The PET results, which used experimental V–T data for the aromatic (C–H) group nonbonded function calibration, does much better with respect to the thermal expansion. It is not obvious why PEN should do less well.

Another observation has to do with the occurrence of a glass transition break in the slope of the V–T curve. It has been found that in a number of cases such a break in the MD generated V–T curve is not far from the experimental T_g.[17] In PET, Fig.1, although there is a change to a lower slope on cooling, the change is rather gradual and the break is not well defined. For PEN the break is seen to be sharper and occurs at $\sim$ 420–430 K. Experimentally, the value is in the range 390–400K [14]. Thus in this case the MD V–T value for T_g is a useful estimate of the experimental one. For both PEN and PET the MD volume reached on cooling into the glass is significantly higher than the experimental glass volumes. This may be due to the high effective cooling rates associated with MD and the rather bulky chemical structures involved.

A volume vs. pressure isotherm (at 597 K) for PEN is shown in Fig. 2 along with comparison results for PET. Experimental results are also included [13,15]. Aside from the obvious vertical displacement of the PEN MD curve from the experimental one due to the zero pressure volume match-up (Fig.1), the PEN MD compressibility fit to the data is about the same as for PET.

The solubility parameter computed as the square-root of the cohesive energy density, is displayed in Fig. 3. The room

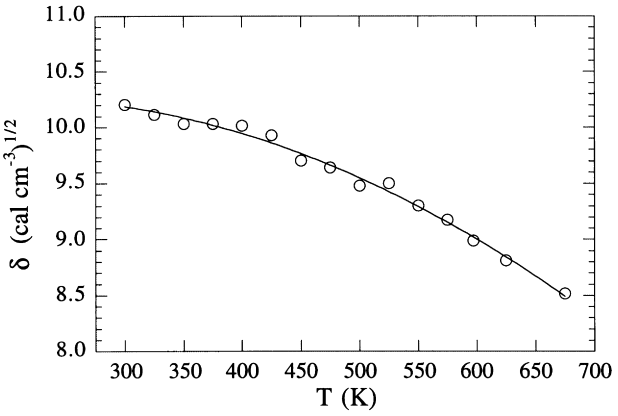

Figure 3. A solubility parameter of PEN vs temperature is determined from MD simulation.

temperature value of 10.2 (cal/cm^3)$^{1/2}$ is virtually identical to the value of 10.3 found for PET [11].

3.2. Diffusion coefficients from simulation

Diffusion coefficients were calculated from the Einstein relation,

$$D = lim\, t \rightarrow \infty \frac{1}{2Ft}\langle |r_i(t) - r_i(0)|^2 \rangle, \quad (1)$$

where D is the self diffusion coefficient of the penetrant, F is the number of dimensions in which the diffusion is occurring ($F = 1,2,3$ for one-, two- and three- dimensional diffusion), t is the time and r_i is the position of the penetrant. The angle brackets refer to averaging accomplished by regarding multiple time points along the trajectory as the starting point at $t = 0$, and also, averaging over more than one penetrant if

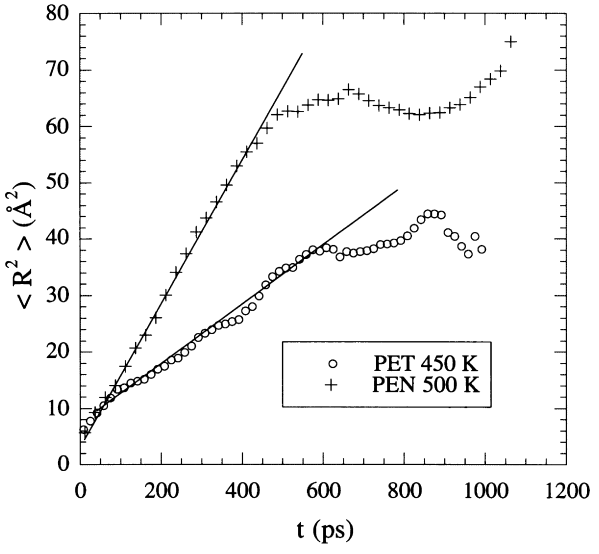

Fig. 4. Diffusion trajectories for methane in PET and PEN at the lowest temperatures employed. The solid lines denote the linear region after the initial cage effect out to the region where the trajectory becomes noisy due to diminishing starting points in multiple starting point averaging.

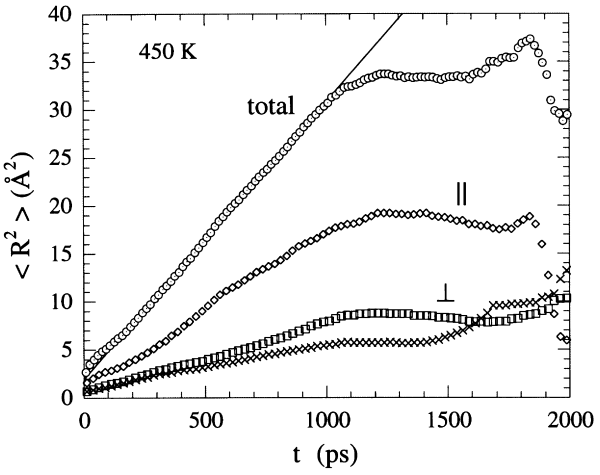

Fig. 5. Diffusion trajectory for methane in 70/30 HBA/HNA LCP at 450 K. The trajectory is also resolved into the components along the chain directions (∥) and transverse to it (⊥).

appropriate. The time interval between origins was selected to be 1 ps. The overall length of the trajectory was dictated by the time taken for clear emergence of linear behavior of $\langle R^2 \rangle$ with time beyond the initial cage effect.

Trajectories, at the lowest temperatures employed, for methane in PET (450 K) and in PEN (500 K) are shown in Fig. 4. In the LCP the diffusant motion is anisotropic and therefore it is of interest to resolve the trajectory into its components with respect to the *a*, *b*, *c* directions of the simulation cell. This is accomplished in Fig. 5 where the mean-square displacements in the direction parallel to the chain alignment (*c* direction) and perpendicular to it (*b*, *c*) are shown. It is apparent that the penetrant progress is considerably faster in the chain direction than in the transverse. It also can be seen that the two transverse directions are largely equivalent. The anisotropy with respect to the parallel and transverse directions obviously confirms the intuitive notion that the diffusant can run along between the chains and parallel to them more easily than it can penetrate the chain cross–sections surrounding it transversely.

Strictly speaking, the diffusion coefficient should be represented for the LCP orthorhombic simulation cell as a 3 × 3 diagonal matrix with components D_a, D_b, D_c. The components are to be calculated separately, using Eq. (1) with $F = 1$, from the three averaged trajectory components; one parallel (*c*) and two perpendicular(*a*, *b*) as in Fig. 5. The spherically averaged diffusion constant, D_{sph}, corresponds to $D_{sph} = (D_a + D_b + D_c)/3$ which is the same result as using the total averaged trajectory $< R^2 >$ in Eq. (1) with $F = 3$. The diffusion coefficient, D, for the LCP will be regarded as the spherically averaged value, D_{sph}.

3.3. Temperature dependence of diffusion constants and comparison with experiment

Inherent in the present work on polymers that are good barrier materials and hence have small diffusion coefficients,

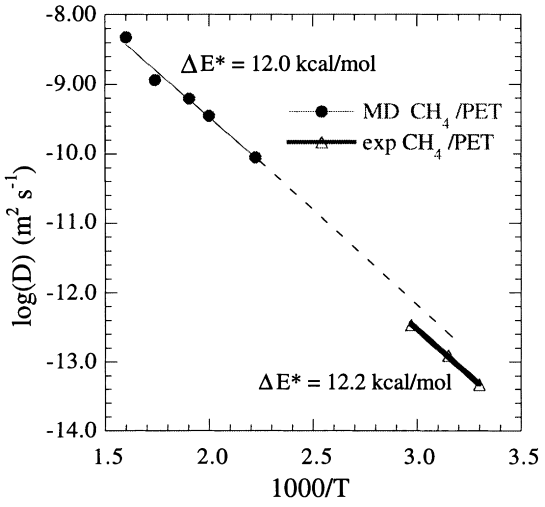

Fig. 6. Log of the diffusion coefficient (D in units of $m^2 s^{-1}$) vs. reciprocal temperature for methane in PET. Results for both MD simulation and experiment [18] are indicated. The dashed line is the extrapolation of the linear regression of the MD points to the region of the experiments. Activation energies are shown on the plot.

is the necessity for the simulations to be carried out well above room temperature in order to generate an adequate diffusant trajectory in practical computation times. Since experimental data tends to be collected near room temperature, this means that considerable extrapolation is necessary to compare the simulations with experiment. Conversely, past experience has shown that the temperature dependence is Arrhenius in nature as long as the mechanism is still largely in the low temperature hopping regime alluded to in the Introduction. This appears to be true even if the glass transition lies in this range. It is therefore of interest to examine this question with the present relatively impermeable polymers. A plot of log D vs. reciprocal temperature for methane self diffusion in PET as determined here via MD simulation is shown in Fig. 6. Also shown is experimental data for methane in amorphous PET [18]. The linear Arrhenius extrapolation of the MD results to the range of the experiments indicates quite reasonable agreement, to within a factor of 2–3 for the diffusion coefficient. The activation energy from MD is very close to the experimental one. Considering the length of the extrapolation, these results are quite encouraging. It also constitutes further evidence that the diffusion behavior remains Arrhenius from above and through the intervening glass transition (experimentally at $\sim$ 450 K in this case). Similar results are shown for PEN in Fig. 7. The only experimental data for PEN located was at one temperature each for oxygen and carbon dioxide as the penetrants [14,19]. Typically, oxygen diffuses several times faster, and carbon dioxide somewhat faster, in polymeric matrices than does methane [1]. Taking this into account, the agreement of simulation with experiment is good.

Turning to the HNA/HBA LCP, the log D vs. reciprocal temperature plot for diffusion of methane from MD is shown in Fig. 8. Comparison with experiment here requires some comment. The polymer created by simulation and considered here corresponds to the polymer in the nematic liquid crystalline state [12]. It remains in this state in simulation on cooling and undergoes vitrification gradually. It is well known experimentally that the nematic state of this polymer undergoes an ordering transition on cooling at $\sim$ 570 K [20–22]. It is accompanied by sharpening of the X-ray diffraction pattern that gives indication of some three dimensional order resulting from translational register of the chains. Sometimes this transition is referred to as

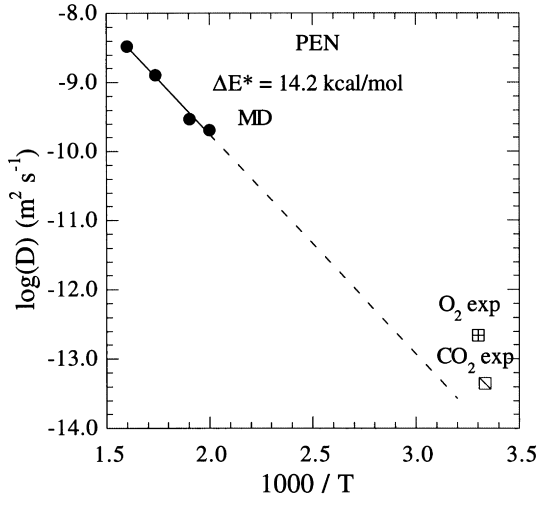

Fig. 7. Log of the diffusion coefficient (D in units of $m^2 s^{-1}$) vs. reciprocal temperature for methane in PEN from MD simulation (filled circles). One experimental point is shown for oxygen [14], and one for carbon dioxide [18] in PEN. The dashed line is the extrapolation of the linear regression of the MD points to the region of the experimental points.

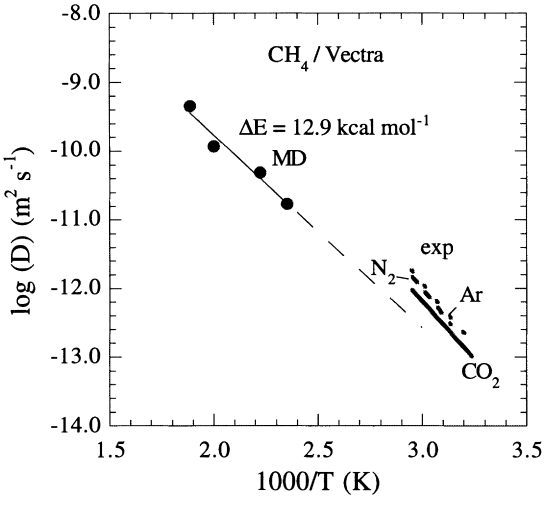

Fig. 8. Log of the diffusion coefficient (D in units of $m^2 s^{-1}$) vs reciprocal temperature for methane in 70/30 HBA/HNA LCP from MD simulation. Also shown, as the heavy lines, is experimental data for argon, nitrogen and carbon dioxide. The dashed thin line is the extrapolation of the linear regression of the MD points to the region of the experimental data.

formation of a 'crystalline' phase. However the heat of fusion and volume change are extremely small [21,22]. The overall degree of order in this random copolymer is obviously far less than that associated with the crystal phase of typical semicrystalline polymers. A reasonable conclusion is that this ordering transition is not likely to result in the dramatic decline in permeability that is typically associated with the crystalline phase compared to the amorphous phase in semicrystalline polymers. Thus the (spherically averaged) diffusion coefficients determined here from simulation are compared directly with the experimental ones.

In Fig. 8, it can be seen that the MD diffusion coefficient for methane in the LCP extrapolates to values just below the experimental values for argon, nitrogen and carbon dioxide [23]. Since methane typically diffuses somewhat slower than any of these gasses [1], it appears that the agreement is satisfactory.

3.4. Mechanism

As in previous work, it is of interest to analyze the trajectories in terms of the type of motions the penetrants undergo. To this end, it is very useful to suppress the penetrant cage motion from the trajectory in order that diffusive jumps may be studied directly. This is conveniently accomplished by a simple filtering process [6]. The trajectory is divided up into a number of equal time intervals, τ. The average position of the penetrant, $\langle r \rangle_\tau$ is computed in each of the intervals, *i*. A replacement trajectory is constructed by connecting the averaged positions. If the interval is selected in the proper range, τ is large enough that the cage motions are largely averaged out but small enough that the diffusive jumps largely remain. This can be tested by comparing the filtered trajectory with the trajectory generated via Eq. (1). With a proper choice of interval, the filtered trajectory follows the latter but with a vertical offset due to the missing cage motion. A diffusive jump is defined as the change of averaged position of the penetrant from one interval to the next. The magnitude of a penetrant jump, $r_p(i)$, from interval $i-1$ to interval i is found from

$$r_p(i)^2 = |\langle r_i \rangle_\tau - \langle r_{i-1} \rangle_\tau|^2 \quad (2)$$

A temporal history, deduced in the manner above, of diffusive jumps is illustrated for methane in the LCP in Fig. 9. Also shown is the trajectory reconstructed from just the diffusive jumps.

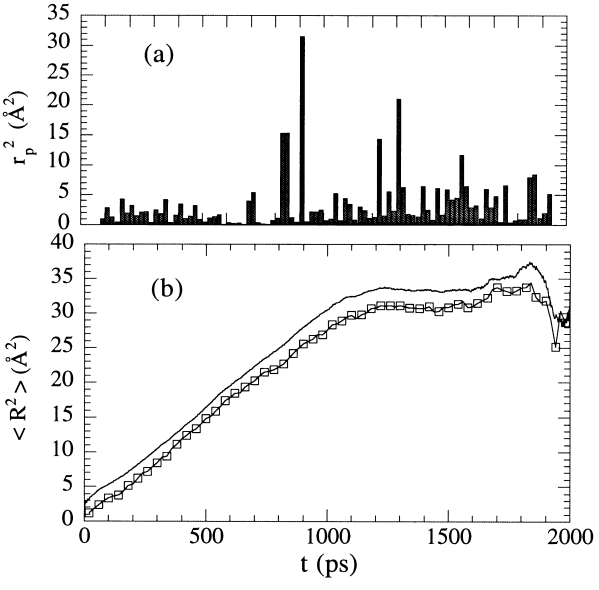

Fig. 9. (a) Temporal history of diffusive jumps for methane in the LCP at 450 K. The squared penetrant displacement r_p^2 is computed between successive positional averages with 20 ps averaging interval. (b) The diffusant trajectory (open squares) reconstructed from the filtered jumps of (a) compared with the actual trajectory (solid curve).

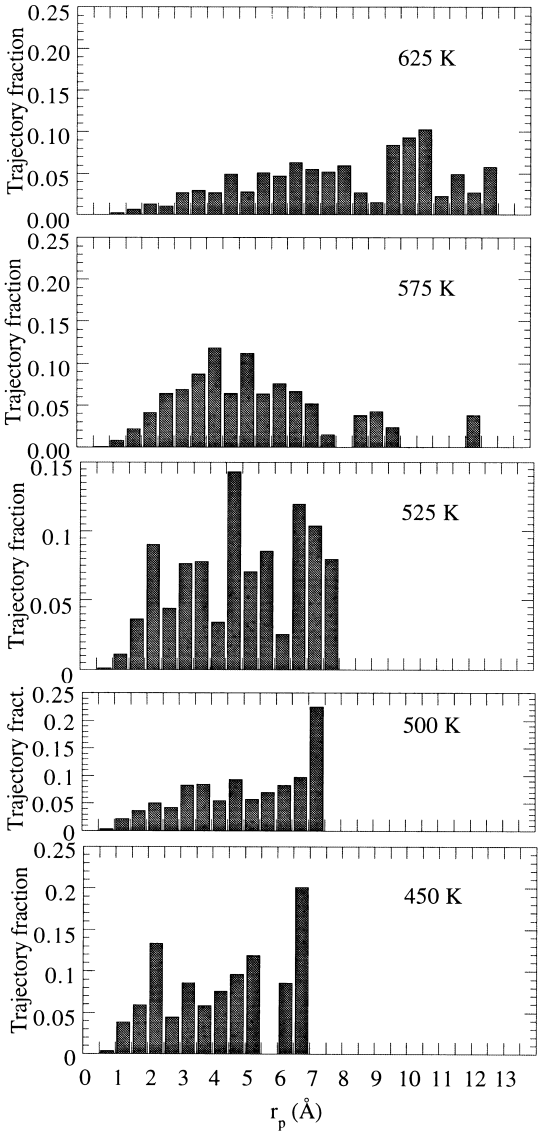

Fig. 10. The contribution of various jump sizes as measured by r_p^2 [see Fig. 9(a)] to the total trajectory for a single methane penetrant in amorphous PET at different temperatures. The averaging interval in the filtering process was 15 ps at 450, 500 and 525 K, 5 ps at 575, 625 K.

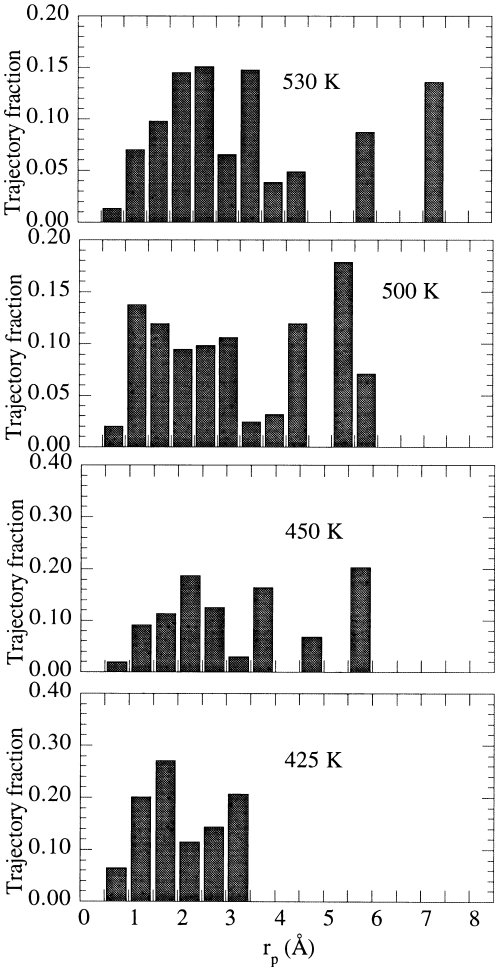

Fig. 11. The contribution of various jump sizes as measured by r_p^2 to the total trajectory for a single methane penetrant in the LCP at different temperatures. The averaging interval in the filtering process was 10 ps at 500 and 530 K, 20 ps at 450 and 425 K.

Since the collection of diffusive jumps is expected to be a random walk the total mean-square penetrant dispacement is given by the sum of the squared jump displacements [6],

$$\langle R^2 \rangle = \sum_i r_p(i)^2 \quad (3)$$

The temporal history of squared diffusive jump magnitudes, r_p^2, as given by Eq. (2), can be sorted in order of size and placed in size interval bins to arrive at a distribution of jump size contributions to the total trajectory. The contribution of various diffusive jump lengths to the trajectory at the temperatures at which diffusion was studied are shown for PET in Fig. 10. The low temperature cage to cage hopping regime is characterized at 450, 500 and 525 K by a distribution that is centered in the region of roughly 4 Å. The latter distance is also approximately the σ diameter of the penetrant. At 575 K the distribution is still largely in this range but has noticeably broadened with some longer jumps now apparent. Finally, the onset of the high temperature regime is evidenced at 625 K by extreme broadening and appearance of very long jumps. This onset at the highest temperature point is not yet seen in the activation energy (Fig. 6). The latter appears to still be Arrhenius with no evidence yet of the high temperature drop-off. The results for PEN, not shown here, are similar to those for PET. The jump length distribution remains in the low temperature regime even at 625 K.

Jump length distributions for the HBA/HNA LCP are shown in Fig. 11. The distributions are all characteristic of the low temperature cage-to-nearby cage hopping regime.

From all of the above, it is to be concluded that the mechanism for all three polymers, as judged from the jump behavior, essentially remains in the low temperature regime over the MD temperature range studied and confirms the reason for success of the Arrhenius extrapolations to near room temperature.

3.5. Free volume correlation

The free volume concept has been widely invoked in interpreting diffusion. From previous simulation results on the hydrocarbon polymers PE, aPP, PIB, *cis*-PBD and aPS it was found [8] that the diffusion coefficient for methane correlated well with the free volume obtained from the simulations. It is of interest to see if such a correlation extends to the polymers studied here. The fractional free volume accessible to a probe sphere of radius, *R*, inserted in the polymer was computed at 400 K for the three polymers investigated. In Fig. 12 the results are compared for these and the five polymers considered previously.

The intercept at $R = 0$ of a curve in Fig. 12, is the total fractional free volume in that polymer. The latter quantity

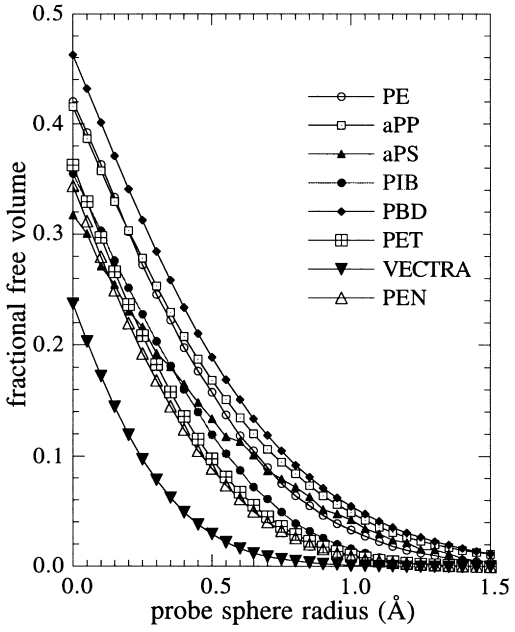

Fig. 12. Fractional free volume distribution with respect to probe sphere radius for different polymeric hosts at 400 K as obtained from MD simulation.

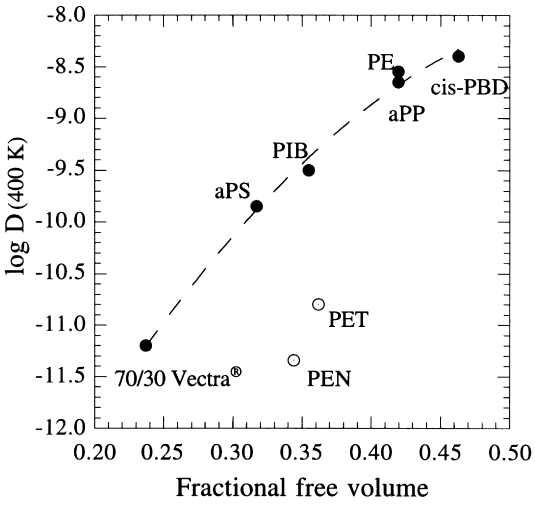

Fig. 13. Diffusion coefficient–fractional free volume correlation map. The logarithm of the diffusion coefficients for methane in different hosts are plotted against the fractional free volumes at 400 K. The dashed curve is a (second order) polynomial fit to the six polymers represented by filled circles. PET, PEN, open circles, do not follow this correlation.

has been used for correlation with the diffusion coefficient at the same temperature, 400 K. The diffusion coefficients at this temperature were determined from the temperature plots of Figs. 6–8. Fig. 13 displays log *D* vs. the fractional free volume at 400 K for the three polymers studied here and the five previous ones.

HBA/HNA LCP appears to fall on the previous correlation curve. It might have been expected that the anisotropic nature of the diffusion would have invalidated any such comparison. The enhancement along the chain direction seems to compensate for the retardation along the transverse directions.

It is very apparent, however, that PET and PEN fall far off the correlation. The diffusion is more than an order of magnitude slower than the free volume correlation would predict. It is interesting to speculate on the structural chemical reasons for the failure of this correlation for PET and PEN. One possibility is that there is 'wasted' free volume in these two polymers. Unlike the other polymers, the chain structure consists of alternating 'thick' sections, made up of bulky aromatic rings, and 'thin' sections, made up of glycol linkages. The packing, as shown by site–site radial distribution functions in PET [11], leads to somewhat open spaces at the glycol linkages that contribute to the fractional free volume. However these regions may be too small to be effective in contributing to promoting penetrant diffusion. Considering the dependence of free volume on probe size is instructive. Returning to Fig. 12, it is noticed that as probe size increases, the curves for PET and PEN rather quickly cross over the ones for PIB and aPS. At 0.5 Å for example, with the exception of vectra the curves do establish the proper order with respect to diffusion coefficient. In any event, perhaps the proper conclusion is that a very simple unadorned notion such as total fractional free volume is not likely to be useful across a wide variety of chemical structures.

Acknowledgements

The authors are indebted to the Polymer Program, Division of Materials Research of the National Science Foundation for financial support of this work. They also acknowledge assistance from the Eastman Kodak Company and are grateful to J.M. O'Reilly and D. Perchak for their interest. The Center for High Performance Computing (CHPC) and the College of Mines at the University of Utah are gratefully acknowledged for use of their computer facilities.

References

[1] Crank J, Park GS, editors. Diffusion in polymers. New York: Academic Press, 1968.
[2] Pant PVK, Boyd RH. Macromolecules 1992;25:494.
[3] Sok RM, Berendsen JC, van Gunsteren WF. J. Chem. Phys. 1992;96:4699.
[4] Mueller-Plathe FJ. Chem. Phys. 1992;96:3200.
[5] Mueller-Plathe F, Rogers SC, van Gunsteren WF. Macromolecules 1992; 25:6722.
[6] Pant PVK, Boyd RH. Macromolecules 1993;26:679.
[7] Han J, Boyd RH. Macromolecules 1994;27:5365.
[8] Han J, Boyd RH. Polymer 1996;37:1797.
[9] Gee RH, Boyd RH. Polymer 1995;36:1435.
[10] Takeuchi H J. Chem Phys 1990;93:2062.
[11] Hedenqvist MS, Bharadwaj R, Boyd RH. Macromolecules 1998;31:1556.
[12] Bharadwaj RK, Boyd RH, Macromolecules, 1998;31:7682.
[13] Walsh DJ, Dee GT. Standard pressure-volume-temperature data for polymers. Lancaster, PA: Technomic, 1995.
[14] Light RR, Seymour RW. Polym Eng Sci 1982;22:857.
[15] Zoller P, Bolli PJ. Macromol Sci. Phys 1980;B18:555.
[16] Coburn JC, Boyd RH. Macromolecules 1986;19:2238.
[17] Han J, Gee RH, Boyd RH. Macromolecules 1994;27:7781.
[18] Michaels AS, Vieth WR, Barrie JA. J Appl Phys 1963;34:13.
[19] Brolly JB, Bower DI, Ward IM. J Polm Sci:Part B: Polym Phys 1996;34:769.
[20] Chivers RA, Blackwell J, Gutierrez GA. Polymer 1984;25:435.
[21] Butzbach GD, Wendorff JH, Zimmermann H. J Makromol Chem Rapid Commun 1985;6:821.
[22] Cao MY, Wunderlich B. J Poly Sci Polym. Phys Ed 1985;23:521.
[23] Chiou JS, Paul DR. J Polym Sci Polym Phys Ed 1987;25:1699.